RANQUE-HILSCH VORTEX TUBE AS AN EDUCATIONAL TOOL FOR CLASSICAL THERMODYNAMICS TEACHING

E. W. Zavaleta-Aguilar[a], B. Narváez-Romo[b,c], and J. R. Simões-Moreira[b]

[a]São Paulo State University (Unesp)
Campus of Itapeva
Department of Engineering
Itapeva 18409-010, SP, Brazil
eli.zavaleta@unesp.br

[b]University of São Paulo
Department of Mechanical Engineering
São Paulo, 05508-900, SP, Brazil
jrsimoes@usp.br

[c]Universidad Pontificia Bolivariana
Facultad de Ingeniería Mecánica
Circular 1 No. 70-01, Medellín, Colombia
betonarmo@usp.br

Received: Oct 16, 2023
Reviewed: Oct 26, 2023
Accepted: Nov 28, 2023

ABSTRACT

A vortex or Ranque-Hilsch tube is a moving parts-free device that splits a compressed air stream into a cold and a hot stream at its two extremities. Although there exist some theoretical approaches based on internal shock and expansion waves as well as Maxwell velocity distribution, a final word on the phenomenon to explain the thermal energy splitting has not been reached yet. Nevertheless, from the classical Thermodynamics point-of-view, the conservation laws of mass and energy along with the Second Law validation applied to a control volume enveloping the vortex must be fulfilled. Consequently, such a simple device may be an outstanding tool for hands-on laboratory teaching of engineering Thermodynamics. In accordance with that, an educational laboratory test rig was conceived to carry out experiments to demonstrate the fundamental laws: mass and energy conservations, and the Second Law constraint. As a secondary goal, students can be acquainted with flow, pressure, and temperature measuring techniques, along with obtaining thermodynamic properties, computing, and data-reducing procedure as part of the testing as well. In addition, the coefficient of performance in refrigeration and heat pump operation modes can be obtained and a proper discussion of the vortex tube working principle can be fostered.

Keywords: thermodynamics laws; vortex tube; Ranque-Hilsch tube; thermal energy splitting; compressed air

NOMENCLATURE

A	area, m2
C_p	specific heat at constant pressure, kJ/(kg.K)
C_v	specific heat at constant volume, kJ/(kg.K)
C_d	discharge coefficient, -
COP	coefficient of performance, -
d	orifice plate hole diameter, m
D	orifice plate tube inner diameter, m
e	relative error, %
h	specific enthalpy, kJ/kg
k	heat capacity ratio, -
L	length, m
M	molar mass, kg/kmol
$\dot{m}$	mass flow rate, kg/s
P	pressure, kPa
R	gas constant, kJ/(kg.K)
R	universal gas constant, kJ/(kmol.K)
Re	Reynolds number, -
s	specific entropy, kJ/(kg.K)
$\dot{S}_g$	entropy generation rate, W/K
T	temperature, ºC, K
V	velocity, m/s
y	molar fraction, -

Greek symbols

β	orifice plate hole diameter to tube inside diameter ratio, -
Δ	difference
ε	expansion factor, -
μ	absolute viscosity, kg/(m.s)
ν	kinematic viscosity, m^2/s
ρ	density, kg/m^3
ϕ	relative humidity, -
ω	specific humidity, -

Subscripts

a	local atmosphere, dry air
c	cold
e	energy
h	hot
HP	heat pump
m	manometric, mass
R	refrigeration
w	water vapor
1	upstream
2	downstream

Superscripts

s saturated

1. INTRODUCTION

Thermodynamics is a fundamental course of any engineering major, especially in Mechanical, Chemical, Electrical, and Civil Engineering as well as in the Energy and Bioengineering field. In thermodynamic courses, it has been noted that students struggle with the challenge of understanding the fundamental conservation laws of mass, energy, and the Second Law of Thermodynamics. Still, there is the difficulty of differentiating processes that take place in a closed system or control volume (open system); therefore, it is necessary to carry out laboratory experimental activities to validate and consequently get acquainted with the theoretical aspects of the fundamental laws. By carrying out a vortex tube experiment, the student will be able to substantiate the veracity of the fundamental laws of Thermodynamics. Therefore, given its importance, it is relevant to introduce the students to a hands-on way of learning its basics, which means carrying out laboratory experiments in well-designed test rigs to assist the learning process. To achieve that, there are several commercial test rigs at some cost, such as Rankine (Gerhart and Gerhard, 2005) and refrigeration (Sun LabTek, 2022) cycles. In this paper, the authors propose using an experimental test rig based on the vortex tube, whose construction is simple and at a low cost. The vortex tube was accidentally invented by G. J. Ranque in 1928 and patented (Ranque, 1934) in the United States in 1934. One decade later, Hilsch (1946) brought the device to a scientific discussion showing its capability for compressed air-cooling purposes. Thus, the device, also known as the Ranque-Hilsch vortex tube or simply RHVT, has the main characteristics of producing both cold and hot air streams from a single compressed air source and being free of moving parts.

In his original work, Ranque (1934) injected a compressed fluid (gas or vapor) tangentially and perpendicular to cylindrical holes bored in a tube. The injected air formed a swirling flow adjacent to the tube's inner wall flowing in the direction of the tube extremities. As the fluid reached a conical obstacle at one tube end, the circumferential aperture between the tube and the obstacle allowed the fluid to discharge into the environment through the annular gap, which, as he noticed, the air was at a higher temperature than that in the inlet stream. Part of the fluid bounced back in the central core to leave at the opposite tube end at a lower temperature than that in the inlet. Therefore, by using this simple device, he produced two air streams at a higher and a lower temperature than that of the compressed air at the inlet. According to Ranque, the fluid in the annular section is subjected to a centrifugal force increasing its pressure and thus its temperature while the fluid in the central part has its pressure decreased and, thus, its temperature. In the same invention, Ranque reported that the vortex tube flows (cold and hot) might be counter-flow or parallel flow as shown schematically in Fig. 1. Whether his explanation correctly describes or not the phenomenon is still a subject of discussion and controversy.

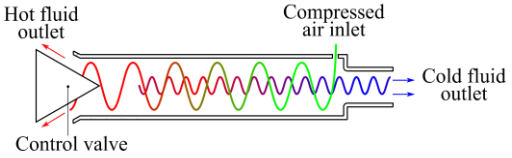

(a) Counter flow type.

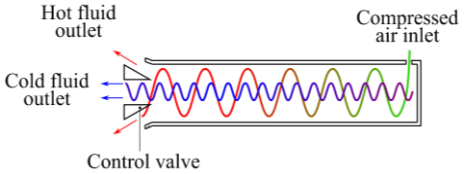

(b) Parallel flow type.

Figure 1. Vortex tube main configurations. (a) counterflow; (b) parallel flow.

Vortex tubes have many applications, such as machining cooling (Aronson, 1976; Liu and Chou, 2007), electronic devices cooling (Sharp et al., 1966; French et al., 2010), vest heating and cooling (Baz and Uhler, 1986; Zhai, 2017), medical applications (Bakhsheshi et al., 2016), natural gas liquefaction (Finko, 1983; Qyyum et al., 2018), water desalination (Terekhin and Zolotykh, 2015), chemical analysis (Bruno, 1994) and gas separation (Stone and Love, 1950; Linderstrøm-Lang, 1964). In gas separation, the vortex tube can work for reducing the CO_2 concentration from natural gas before combustion (Rafiee, 2023) or CO_2 capture from the air (Yun et al., 2018).

The fundamental working principle is not totally understood yet (Simões-Moreira, 2010). Nevertheless, it is worthwhile to mention that although a not complete understanding of the phenomenological operating aspects has been achieved successfully, the fundamental conservation laws of mass and energy as well as the Second Law of Thermodynamics applied to the control volume around the vortex must be fulfilled. So, this work aims to have a laboratory device so the students can demonstrate those laws in a vortex tube for hands-on teaching purposes in classical Thermodynamics courses. Furthermore, students can practice collecting and measuring raw data, such as pressure, temperature, and flow rate, to reduce further them into proper ways for analysis and the conservation laws validation.

2. CONSERVATION LAWS FOR THE RHVT

In Fig. 2, there is a diagram of an RHVT. Considering a steady state, adiabatic process, the three conservation laws of the process to the RHVT are indicated as follows:

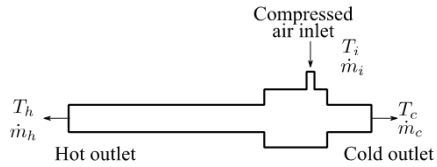

Figure 2. Vortex tube scheme for the analysis of conservation laws.

Mass conservation:

$$\dot{m}_i = \dot{m}_h + \dot{m}_c \quad (1)$$

In that, $\dot{m}_i$ is the inlet air mass flow rate measured at the orifice plate and, $\dot{m}_h$ and $\dot{m}_c$ are the hot and cold outlet mass flow rates, respectively. The mass conservation of Eq. (1) must also be analyzed considering the measuring uncertainties, by introducing the mass conservation relative error, e_m, which can be evaluated from Eq. (2).

$$e_m = \frac{\dot{m}_i - (\dot{m}_h + \dot{m}_c)}{\dot{m}_i} \times 100\% \quad (2)$$

Energy conservation:

The overall energy balance neglects the kinetic and potential contributions because they are negligible (in this case, less than 0.01%). Consequently, steady-state energy conservation can be expressed as shown in Eq. (3):

$$\dot{m}_i h_i = \dot{m}_h h_h + \dot{m}_c h_c \quad (3)$$

where h_i, h_h and h_c are the specific enthalpy of the air at the inlet and hot and cold outlet respectively. The energy conservation relative error, e_e, can be evaluated from Eq. (4):

$$e_e = \frac{\dot{m}_i h_i - (\dot{m}_h h_h + \dot{m}_c h_c)}{\dot{m}_i h_i} \times 100\% \quad (4)$$

Second Law constraint:

The rate of entropy generation, $\dot{s}_g$, in steady state, without heat transfer with the environment, accounts only for the internal irreversibility and is given by Eq. (5).

$$\dot{s}_g = \dot{m}_h s_h + \dot{m}_c s_c - \dot{m}_i s_i \quad (5)$$

Where s_i is the air inlet specific entropy. The Second Law of Thermodynamics is fulfilled for $\dot{s}_g \geq 0$, is equal to zero for reversible processes and positive for irreversible (real) processes, such as it takes place in an RHVT.

3. DESCRIPTION OF THE EXPERIMENTAL SETUP

The schematics in Fig. 3 detail the actual experimental setup in current use in the laboratory, which is also shown in a still picture in Fig. 4. To reduce pressure fluctuations, the compressed feeding line has a receiver tank. Next, the compressed air feeds a pressure regulation valve, coupled with a water trap air filter, where the inlet pressure and air mass flow can be adjusted. Once established the steady-state flow regime, the compressed air mass flow rate that flows into the device is m ̇_i, which is evaluated by measuring the pressure drop (ΔP) over an orifice plate mounted in a rectifying pipe. The local atmospheric pressure (P_a) is obtained from a barometer reading. The pressure drop across the orifice plate is obtained from direct readings of a U-tube water column manometer; the inlet compressed air temperature is obtained from a calibrated K-type thermocouple. After all readings (pressure, temperature, and pressure drop), it is possible to evaluate the inlet compressed air mass flow rate. The rectifying pipe length before and after the orifice plate follows the recommendation of ASME standard MFC-3M-2004 (ASME, 2004).

As the compressed air reaches the vortex generator, it is split into two flow streams, one colder and the other hotter than the inlet compressed air. The two exit tubes are coupled to two different thermally insulated rectifying tubes provided with flow and temperature measuring stations as illustrated in Fig. 3 and also shown in the still picture in Fig. 4.

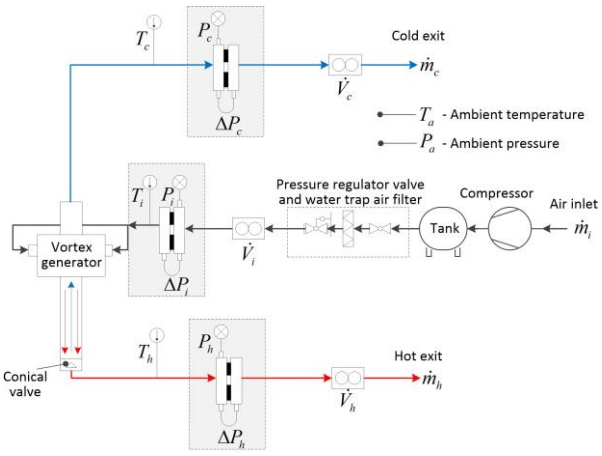

Figure 3. Vortex tube setup scheme.

The two exit flow temperatures (hot and cold lines) were obtained from calibrated K-type

thermocouples installed in the pipes. Two standard orifice plates were mounted at the hot and cold tubes to obtain their mass flow rates. The static pressures upstream of the orifice plates (hot and cold lines) were obtained from Bourdon pressure gauges. Pressure drops across the orifice plates were measured using U-tube water column manometers.

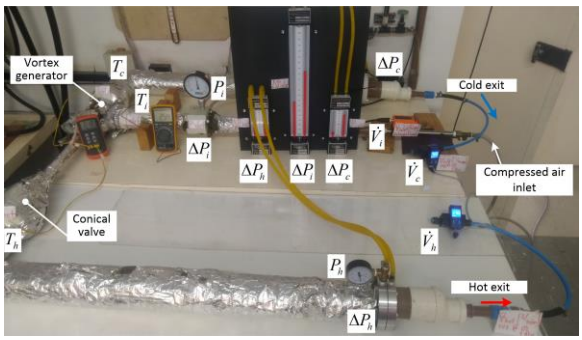

Figure 4. Experimental setup still picture.

All experimental circuit tubing and parts walls were thermally insulated with 22 mm mineral wool, as can be seen in Fig. 4.

3.1. The vortex tube

The counter-flow vortex tube device used in this work includes a vortex generator device, and two pieces of tubes located at both sides of the vortex generator (see Fig. 5). The vortex generator may have more than one inlet (in this work there are two inlets). The inlet holes are tangential to the inner tube wall. As the device name suggests, the vortex generator produces fluid vortices that flow inside the longer tube, which has a conical valve mounted at its end. Such a valve allows one to vary the exiting hot mass flow rate. As the flow reaches the valve, part of the fluid returns back around the centerline, also forming a counter-flow vortex, that exits at another shorter piece of tube located at the opposite part of the vortex generator.

(a) Vortex tube still picture.

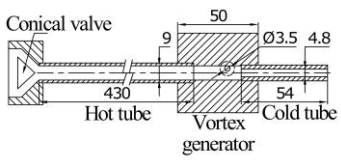

(b) Vortex tube scheme (lengths in mm).

Figure 5. Vortex tube. (a) still picture; (b) construction details.

3.2. Fundamental instrumentation

Fundamental instrumentations were used for measuring raw data, such as temperature and pressure. Given the instructive goal of this work, working equations for obtaining reduced data are presented next to facilitate the implementation of this device as a learning tool. Magnitude values can be attained by using stand-alone instruments, as in this work, or by using a data acquisition system.

3.2.1. Orifice plate mass flow rate

Three standard orifice plates were installed in the vortex tube: at the inlet compressed air line, and the cold and hot air exit circuits, as can be seen in Figs. 2 and 3, which provide raw data to indirectly obtain the mass flow rate for each circuit. The flanges, orifice plates, and upstream and downstream tube lengths were manufactured following ASME standard MFC-3M-2004 (ASME, 2004). The air inlet orifice plate was made out of stainless steel and their flanges of nylon; a still picture and a schematic of them are shown in Figs. 5a and 5b. The hot and cold lines orifice plates were manufactured in ABS (Acrylonitrile Butadiene Styrene) plastic by using a 3D printer, as depicted in Fig. 6c. These two orifice plates were placed into stainless steel flanges (Fig. 6d). The equations for calculating the mass flow rate are presented in Appendix A. In place of orifice plates, commercial equipment to directly measure volumetric or mass flow can be used as well.

3.2.2. Temperature measurements

For temperature measurements were used K-type thermocouples installed in ¼" NPT threaded holes. The thermocouples were calibrated for a range from -10°C to 35°C by using a temperature calibration bath PRESYS T-25N. Other thermocouple types can be used, even, PT-100 or any other temperature sensor. Four temperature stations are necessary as indicated in Fig. 3. The first one indicates the local ambient temperature (T_a); the second one, the orifice plate upstream compressed air temperature (T_i); the third and the fourth ones, the hot (T_h) and cold (T_c) air flow temperatures.

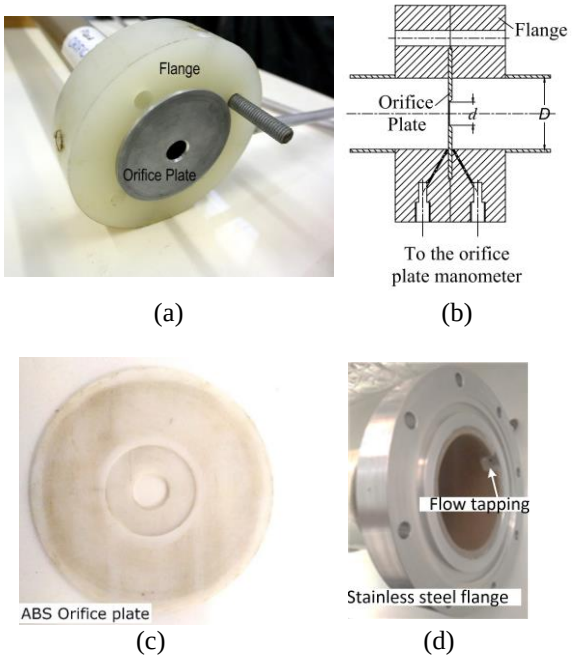

Figure 6. Orifice plates and flanges. (a) Inlet orifice plate still picture; (b) Orifice plate scheme; (c) Cold and hot ABS orifice plates still picture; (d) Cold and hot orifice plate stainless steel flange still picture.

3.2.3. Pressure measurements

Two types of pressure gauges (Bourdon and U-tube) were used along with a barometer that provided the local atmospheric pressure (P_a). The three Bourdon gauges were calibrated from 100 kPa to 400 kPa range by using a pressure calibrator PRESYS PC-5047. The Bourdon manometers indicate the air gauge pressures (P_m) being installed at the inlet, hot, and cold upstream orifice plates (Figs. 3 and 4). The absolute pressure (P) was evaluated by Eq. (6):

$$P = P_a + P_m \quad (6)$$

Finally, three U-tube manometers, one in the -100 to 100 mmWC range (inlet line) and two in the -50 to 50 mmWC range (cold and hot lines) were used. This pressure gauge type was installed at each orifice plate (inlet, hot, and cold) as indicated in Fig. 3. The pressure drop was directly acquired from the instrument reading. A still picture of the U-tube manometers used is shown in Fig. 4.

3.2.4. Humid air considerations

At the local conditions, the inlet vortex tube compressed air relative humidity is 60%. Due to the low temperature at the vortex tube cold exit, the humid air was considered saturated, that is, its relative humidity is 100%. The hot exit line relative humidity was obtained from a mass balance between the inlet and cold lines. The thermophysical property assessments consider a dry air and water vapor mixture and their mixing rules are detailed in Appendix B.

4. DATA REDUCTION AND RESULTS

Some geometrical and constructive parameters of the test section shown in Section 3.2.1 are also presented in Table 1. The table also indicates the error propagation and measurement uncertainties in the last column.

Table 1. Orifice plates parameters and magnitudes of the test rig tested.

Parameter	Variable	Value
Orifice plate tube inside diameter – inlet	D_i (m)	$(43.4 \pm 0.2) \times 10^{-3}$
Orifice plate hole diameter – inlet	d_i (m)	$(14.1 \pm 0.2) \times 10^{-3}$
Orifice plate hole diameter to inside tube diameter ratio – inlet	β_i (-)	0.3249 ± 0.004
Orifice plate tube inside diameter – hot and cold	D_h, D_c (m)	$(65.9 \pm 0.2) \times 10^{-3}$
Convergent nozzle hole diameter – hot and cold	d_h, d_c (m)	$(16.9 \pm 0.2) \times 10^{-3}$
Orifice plate hole diameter to inside tube diameter ratio – hot and cold	β_h, β_c (-)	0.2564 ± 0.004

Next, the main raw data were collected as the given example in Table 2 (the complete dataset can be found Zavaleta-Aguilar et al. 2023). Data were obtained from instrument readings as described in previous sections. It is advised that the students should repeat the data collection at least three times and cast the average value in the last column of that table. It is suggested to carry out the experiment for at least three inlet pressures so that the overall trend can be captured.

Table 2. Measurements of the RH-4 test performed – raw data.

Parameter	Variable	Value
Orifice plate upstream air gauge pressure - inlet	$P_{m,i}$ (kPa)	255.0 ± 2.5
Orifice plate upstream air gauge pressure – hot line	$P_{m,h}$ (kPa)	49.0 ± 2.5
Orifice plate upstream air gauge pressure – cold line	$P_{m,c}$ (kPa)	49.0 ± 2.5
Atmospheric pressure	P_a (kPa)	93.4 ± 0.1
Orifice plate air pressure difference – inlet	ΔP_i (kPa)	1.4210 ± 0.0098
Orifice plate air pressure difference – hot line	ΔP_h (kPa)	0.6370 ± 0.0098
Orifice plate air pressure difference – cold line	ΔP_c (kPa)	0.1863 ± 0.0098

Air inlet temperature	T_i (ºC)	24.0 ± 0.2
Hot line air temperature	T_h (ºC)	31.9 ± 0.2
Cold line air temperature	T_c (ºC)	10.0 ± 0.2

Now, the students face the task of reducing the data to demonstrate the conservation laws given in Section 2. Some processed data are given in Table 3 for the RH-4 test to evaluate the inlet, hot and cold lines mass flow rate. A detailed procedure to obtain the mass flow uncertainty propagation is indicated in Appendix C.

Table 3. Inlet, hot, and cold orifice plates reduced data parameters for the RH-4 test sample experiment, whose values are presented in Table 2.

Parameter	Var.	Inlet	Hot exit	Cold exit
Absolute pressure	P (kPa)	348.4 ± 2.5	142.4 ± 2.5	142.4 ± 2.5
Air density	ρ (kg/m^3)	4.075 ± 0.029	1.624 ± 0.029	1.746 ± 0.031
Reynolds number	Re_D (-)	16437 ± 368	6385 ± 137	3829 ± 125
Discharge Coeff*	C_d (-)	0.6096 ± 0.0001	0.6068 ± 0.0001	0.6100 ± 0.0002
Expansion factor*	ε (-)	0.99897 ± 0.00001	0.99887 ± 0.00003	0.99967 ± 0.00002
Mass flow rate	$\dot{m}$ (kg/s)	(10.3 ± 0.2)×10^{-3}	(6.2 ± 0.1) ×10^{-3}	(3.5 ± 0.1) ×10^{-3}

*In thermodynamic laboratory practices, it is suggested that the discharge coefficient values (C_d) and the expansion factor (ε) should be previously provided to students.

The inlet line orifice plate upstream air absolute pressure is evaluated according to Eq. (6), obtaining P_i = 348.4 kPa. That pressure along with the inlet temperature T_i = 24.0 ºC one obtains the air density ρ_i = 4.075 kg/m^3 (Eq. (B.1)) and k = 1.399 (Eq. (B.12)). According to the Table 2, the inlet orifice plate pressure drop is ΔP = 1.421 kPa. To evaluate the mass flow rate (Eq. (A.1)) is required the discharge coefficient, C_d (Eq. (A.2)), that depends on the Reynolds number, Re_D (Eq. (A.6)), that depends on the velocity V which is unknown, so this value will be assumed at the outset. Assuming V = 1.71 m/s it is found Re_D = 16437, C_d = 0.6096, ε = 0.99897 (Eq. (A.7)) and $\dot{m}$ =0.0103 kg/s. With the calculated mass flow rate, the inlet velocity can be evaluated from Eq. (7).

$$V = \frac{4\dot{m}}{\rho\pi D^2} \tag{7}$$

For the given example, the calculated velocity is V = 1.71 m/s, which is equal to the velocity initially assumed. If the calculated velocity were different, an iterative solution process is necessary to achieve a better approximation, for example, the algorithm outlined in Fig. 7.

Similarly, the hot and cold fluid results are shown in Table 3. Table 4 shows the mass flow rates evaluated, as well as their relative errors (Eq. (2)) for the 4 tests performed as a function of different absolute inlet pressures. It can be noted in Table 4 that the mass maximum relative error is in the test RH-4, with a value of 5.8%.

Table 5 shows the energy balance components of the First Law of Thermodynamics, and the energy balance errors (Eq. (4)). The specific enthalpy for each line was evaluated by Eq. (B.19). As can be seen in Table 5, the energy balance is fulfilled, with a maximum error of 5.6%. This happen because the system was correctly thermally insulated avoiding walls heat losses or gains.

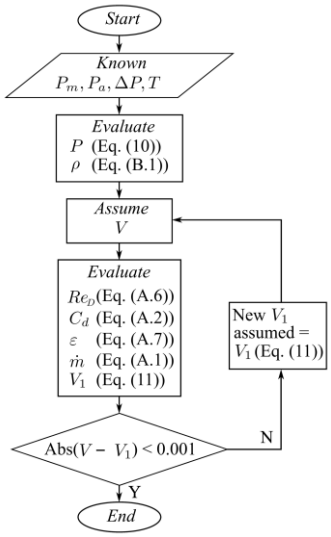

Figure 7. Velocity iterative calculation algorithm scheme for a given orifice plate.

Table 4. Mass flow rates and mass balance relative errors according to Eq. (2).

Test code	P_i (kPa)	$\dot{m}_i$ (kg/s)	$\dot{m}_h$ (kg/s)	$\dot{m}_c$ (kg/s)	e_m (%)
RH-1	216.0	0.0059	0.0037	0.0020	3.0
RH-2	255.2	0.0072	0.0046	0.0026	0.3
RH-3	314.1	0.0092	0.0058	0.0032	1.8
RH-4	348.4	0.0103	0.0062	0.0035	5.8

Table 5. Energy conservation and their relative errors (Eq. (4)).

Test code	$\dot{m}_i h_i$ (W)	$\dot{m}_h h_h$ (W)	$\dot{m}_c h_c$ (W)	e_e (%)
RH-1	234.7	154.1	72.94	3.3
RH-2	268.2	190.1	77.71	0.1
RH-3	321.1	231.3	85.81	1.2

RH-4	332.3	231.7	82.15	5.6

In the case of the Second Law of Thermodynamics (Eq. (5)), it is verified, according to Table 6, positive entropy generation rate values which means that the measurements of the experiments are coherent and indicate that the device is irreversible as one would expect.

In addition, by analyzing a thermodynamic air-standard cycle for the Ranque-Hilsch tube (Simões-Moreira, 2010), the coefficient of performance (COP) was evaluated for refrigeration (COP_R) and heat pump (COP_{HP}) operation modes. These coefficients are defined by the Eqs. (8) and (9), respectively:

Table 6. Entropy generation rate according to Eq. (5).

Test code	$\dot{m}_i s_i$ (W/K)	$\dot{m}_h s_h$ (W/K)	$\dot{m}_c s_c$ (W/K)	$\dot{S}_g$ (W/K)
RH-1	-0.4442	0.4314	0.2020	1.08
RH-2	-0.9400	0.3193	0.0861	1.35
RH-3	-1.8287	0.2499	0.0022	2.08
RH-4	-2.4578	0.2121	-0.0384	2.63

$$COP_R = \frac{\dot{m}_c}{\dot{m}_i}\frac{k}{k\text{-}1}\left[\frac{1\text{-}T_c/T_i}{\ln(P_i/P_a)}\right] \quad (8)$$

$$COP_R = \frac{\dot{m}_h}{\dot{m}_i}\frac{k}{k\text{-}1}\left[\frac{T_h/T_i - 1}{\ln(P_i/P_a)}\right] \quad (9)$$

In Eqs. (8) and (9) the temperatures are the absolutes ones (K). It was theoretically demonstrated by Simões-Moreira (2010) that under ideal conditions the refrigeration and heat pump coefficients of performance should be equal. This fact is shown in Table 7 for the 4 tests performed at different mass flow rates and pressures, where a maximum difference of 4% was found between these COPs. Although those values are up to 100 times lower than conventional compression refrigeration systems, specific applications of vortex tubes might be investigated. Moreover, the COPs equality condition between the refrigeration and the heat pump modes operation can be used as a double check of the laws of conservation of mass and energy applied to an air-standard cycle.

Table 7. Ranque-Hilsch coefficient of performance for refrigeration (COP_R) and heat pump (COP_{HP}) modes operation (Eqs. (8) and (9)).

Test code	COP_R	COP_{HP}	e_{COP} (%)
RH-1	0.0551	0.0522	5.2
RH-2	0.0526	0.0531	1.0
RH-3	0.0460	0.0476	3.5
RH-4	0.0429	0.0422	1.5

The results indicate that both the entropy generation rate (Table 6) and the coefficient of performance (Table 7) are strongly affected by the operating conditions. An entropy generation rate of 2.63 W/K was evaluated in the RH-4 test, which was about twice the value obtained in the RH-1 test. The COP of the RH-4 test was lower than that of the test RH-1, indicating that, the higher the entropy generation rate, the lower the COP. These findings suggest that research for improving the thermal efficiency in vortex tubes should focus on reducing the entropy generation rate using passive and active techniques, as mentioned in Awais and Bhuiyan (2018).

5. CONCLUSIONS

A simple RHVT was conceived and tested aiming to demonstrate the fundamental laws of classical Thermodynamics to become an instructive tool for undergraduate students to get acquainted with those laws in a practical laboratory experiment. A test rig and a typical experimental procedure were presented. Tests were performed to demonstrate the validation of mass conservation along with the First and Second Laws of Thermodynamics. As a secondary goal, the students also become familiar with flow, pressure, and temperature measuring techniques and instruments.

The results indicate that for the performed tests in this work, there is a maximum relative error in the mass conservation of 5.8% and the energy conservation of 5.6% for the specifically conceived test rig. The positive entropy generation rate $\dot{S}_g$ shows that there are irreversibilities, as one would expect in such a device and, therefore, the students can demonstrate that the Second Law of Thermodynamics is also fulfilled. In addition, the vortex tube coefficient of performance for refrigeration and heat pump modes was evaluated, demonstrating experimentally that these values are equal, given in this work a maximum relative error of 5.2% in the tests.

Due to its high processing load, the experiment can be seen throughout the discipline, so at the beginning, the temperatures and pressures can be measured, in a second time the mass flow rates can be evaluated together with the law of conservation of mass, after the evaluating the properties thermodynamics such as enthalpy and entropy and finally verify the first law of thermodynamics and the Second Law constraint.

Finally, we hope that the RHVT test rig can be combined with other subjects such as psychrometry, instrumentation, data reduction, and error propagation analysis. Also, the device can be a motivation for students to search for the answer to explain the device operation principle.

ACKNOWLEDGEMENTS

The authors would like to thank the Sao Paulo Research Foundation (FAPESP) for the project funding - Grant No. 2016/09509-1. Moreover, the

second author thanks FAPESP for the personal financial support - Grant No. 2020/08211-4, as well as the Colombian Administrative Department of Science, Technology and Innovation -Minciencias - (COLCIENCIAS grant 1.087.046.934-728/2015).

Appendix A. Calculation of mass flow rate by using orifice plates

The mass flow principle is based on the Bernoulli equation applied to the downstream and upstream sections of an orifice plate (Fig. 6). The mass flow rate is corrected by the discharge coefficient (C_d) and the expansion factor (ε) which consider the fluid contraction at the hole plate exit and pressure losses due to irreversibility. Thereby, the inlet air mass flow rate is evaluated according to Eq. (A.1).

$$\dot{m} = \frac{C_d \varepsilon A_2}{\sqrt{1-\beta^4}} \sqrt{2\rho_1 \left(P_1 - P_2\right)} \quad (A.1)$$

Where, $A_2 = \pi d^2/4$ is the hole plate cross-section area, $\beta = d/D$ is the hole diameter to the tube inside diameter ratio, P_1 and P_2 are the orifice plate upstream and downstream pressures, respectively. The air density in section 1 is evaluated from the ideal equation-of-state for the measured values of P_1, T_1, and relative humidity (Eq. B.1). The installed orifice plates (inlet, hot and cold lines) are concentric conical outlet type with hole diameter d and tube inside diameter D. The discharge coefficient for corning tapping is evaluated by Eq. (A.2) (Reader-Harris and Sattary, 1996):

$$C_d = 0.5961 + 0.0261\beta^2 - 0.216\beta^8 + 0.000521(10^6 \beta Re_D)^{0.7} + (0.0188 + 0.0063A)\beta^{3.5}(10^6 Re_D)^{0.3} + (0.043 + 0.080e^{(-10L_1)} - 0.123e^{(-7L_1)})(1-0.11A)\beta^4(1-\beta^4) - 0.031(M_2' - 0.8M_2'^{1.1})\beta^{1.3} \quad (A.2)$$

In case of D < 71.12 mm it should be added to Eq. (A.2) the amount: $+0.011(0.75-\beta)[2.8-(D/25.4)]$, D should be given in mm. In Eq. (A.2) the parameters A, M_2' ,and L_1 are:

$$A = (19000\beta/Re_D)^{0.8} \quad (A.3)$$

$$M_2' = 2L'_2/(1-\beta) \quad (A.4)$$

$$L_1 = L'_2 = 0 \quad (A.5)$$

The Reynolds number is evaluated according to Eq. (A.6):

$$Re_D = VD/v \quad (A.6)$$

Wherein, v is the air kinematic viscosity at section 1 and V is the mean air velocity inside the tube with diameter D (see Fig. 6b). The expansion factor (ε) for corning tappings and $P_2/P_1 \geq 0.75$ conditions, can be calculated according to Eq. (A.7) (Reader-Harris, 1998).

$$\varepsilon = 1-(0.351+0.256\beta^4+0.930\beta^8)[1-(P_2/P_1)^{(1/k)}] \quad (A.7)$$

Wherein, k is the heat capacity ratio in section 1, defined in Eq. (B.12).

Appendix B. Thermophysical properties

Although data reduction of thermophysical properties might be easily computed by using the ideal gas law assumption, authors strongly suggest the use of the thermophysical properties following mixing rules of dry air and water vapor, which are detailed below.

B.1 Density

The humid air density is evaluated by Eq. (B.1)

$$\rho = PM/\left(R\left(T+273.15\right)\right) \quad (B.1)$$

$$M = y_a M_a + y_w M_w \quad (B.2)$$

Where, R =8.314 kJ/(kmol.K) is the universal ideal gas constant, y_a and y_w are the dry air and water vapor mole fraction, respectively, M_a = 28.9583 kg/kmol and M_w = 18.015 kg/kmol are the dry air and water vapor molar mass, respectively and M is the mixture molar mass. It is possible to evaluate the water vapor molar fraction (y_w) from the specific humidity (ω). The latter is defined as the water vapor mass to dry air mass ratio,

$$y_w = \omega M/(1+\omega)M_w \quad (B.3)$$

$$y_a = 1-y_w \quad (B.4)$$

The specific humidity is defined by Eq. (B.5) (Kuehn et al., 1998):

$$\omega = 0.622(\phi P_w^s)/(P+\phi P_w^s) \quad (B.5)$$

In which, ϕ is the relative humidity, P is the humid air pressure and P_w^s is the saturated water pressure at the humid air temperature.

B.2 Specific heat

The air and water vapor specific heat ($C_{p,a}$, $C_{p,w}$) (Borgnakke and Sonntag, 2019) and the humid air specific heat (C_p) (Wong and Embleton, 1984) are evaluated by:

$$C_{p,a} = 1.05 - 0.365\theta + 0.85\theta^2 - 0.39\theta^3 \quad \text{(B.6)}$$

$$C_{p,w} = 1.79 + 0.107\theta + 0.586\theta^2 - 0.2\theta^3 \quad \text{(B.7)}$$

$$\theta = (T + 273.15)/1000 \quad \text{(B.8)}$$

$$C_p = C_{p,a} y_a M_a / M + C_{p,w} y_w M_w / M \quad \text{(B.9)}$$

B.3 Specific heat ratio

$$C_v = C_p R \quad \text{(B.10)}$$

$$R = \Re / M \quad \text{(B.11)}$$

$$k = C_p / C_v \quad \text{(B.12)}$$

A more precise definition of humidity parameters based on real gas mixtures can be found (Simões-Moreira, 1999).

B.4 Absolute viscosity

The air and water vapor viscosities (μ_a, μ_w) (Kleiber and Joh, 2010) and the humid air absolute viscosity (μ) (Wilke, 1950) were evaluated according to:

$$\mu_a = -0.0172\times10^{-5} + 0.79965\times10^{-7}(T+273.15) - 0.72183\times10^{-10}(T+273.15)^2 + 0.0496\times10^{-12}(T+273.15)^3 - 0.01388\times10^{-15}(T+273.15)^4 \quad \text{(B.13)}$$

$$\mu_w = 0.64966\times10^{-5} - 0.15102\times10^{-7}(T+273.15) + 1.15935\times10^{-10}(T+273.15)^2 - 0.1008\times10^{-12}(T+273.15)^3 + 0.031\times10^{-15}(T+273.15)^4 \quad \text{(B.14)}$$

$$\mu = (y_a\mu_a)/(y_a\Phi_{aa} + y_w\Phi_{aw}) + (y_w\mu_w)/(y_a\Phi_{wa} + y_w\Phi_{ww}) \quad \text{(B.15)}$$

$$\Phi_{aa} = \Phi_{ww} = 1 \quad \text{(B.16)}$$

$$\Phi_{aw} = [1 + (\mu_a/\mu_w)^{1/2}(M_w/M_a)^{1/4}]^2 / [8(1 + M_a/M_w)]^{1/2} \quad \text{(B.17)}$$

$$\Phi_{wa} = [1 + (\mu_w/\mu_a)^{1/2}(M_a/M_w)^{1/4}]^2 / [8(1 + M_w/M_a)]^{(1/2)} \quad \text{(B.18)}$$

B.5 Specific enthalpy

The humid air specific enthalpy by humid air mass unit was evaluated by Eq. (B.19) (Kuehn et al., 1998):

$$h = \left[C_{p,a}\, T + \omega(2501 + C_{p,w}\, T)\right]/(1+\omega) \quad \text{(B.19)}$$

B.6 Specific entropy

The humid air specific entropy by humid air mass unit was evaluated by Eq. (B.20) (Kuehn et al., 1998):

$$s = \left[\left(C_{p,a} + \omega C_{p,w}\right)\ln\left((T+273.15)/(T_0+273.15)\right) - R_a \ln\left(P_a/P_0\right) + \omega\left(6.7975 - R_w \ln\left(P_w/P_0\right)\right)\right]/(1+\omega) \quad \text{(B.20)}$$

Where the reference state is T_0 = 0 °C and P_0 = 101.325 kPa. Furthermore, the water state is saturated liquid. R_a = 0.287 kJ/(kg.K) and R_w = 0.462 kJ/(kg.K) are the particular gas constants and P_a and P_w, the dry air and water vapor partial pressures, respectively. Finally, it is worthwhile to mention that thermophysical properties can alternatively be computed by using, for instance, Engineering Equation Solver software or by importing packages in high-level programming languages such as Coolprop package being imported in Python, and so on.

Appendix C. Uncertainty Analysis

The inlet air mass flow rate uncertainty propagation of the RH-4 test is indicated below. The mass flow is evaluated according to Eq. (C.1). In this equation one notices that the independent variables are as shown in Eq. (A.1).

$$\dot{m} = \dot{m}(d, D, V, T, P_m, \Delta P, P_a) \quad \text{(C.1)}$$

Thus, the mass flow uncertainty ($\sigma_{\dot{m}}$) is evaluated by:

$$\sigma_{\dot{m}}^2 = \left[(\partial\dot{m}/\partial d)\sigma_d\right]^2 + \left[(\partial\dot{m}/\partial D)\sigma_D\right]^2 + \left[(\partial\dot{m}/\partial V)\sigma_V\right]^2 + \left[(\partial\dot{m}/\partial T)\sigma_T\right]^2 + \left[(\partial\dot{m}/\partial P_m)\sigma_{P_m}\right]^2 + \left[(\partial\dot{m}/\partial P)\sigma_P\right]^2 + \left[(\partial\dot{m}/\partial P_a)\sigma_{P_a}\right]^2 \quad \text{(C.2)}$$

Initially, the velocity uncertainty (σ_V) is unknown, so this value is assumed, later verified using the uncertainty analysis of Eq. (7). Table C.1 indicates the partial derivative and the uncertainty values of each independent variable.

Table C.1. Partial derivative and the uncertainties of each mass flow rate independent variable (x_i) for the RH-4 test inlet air mass flow rate.

	x_i						
	d	D	V	T	P_m	ΔP	P_a
$\frac{\partial\dot{m}}{\partial x_i}$	1.478	-0.011	-3.5×10^{-5}	-1.7×10^{-5}	1.4×10^{-5}	3.6×10^{-3}	1.5×10^{-5}
Unit	kg/(s.m)	kg/(s.m)	kg/m	kg/(s.°C)	kg/(s.kPa)	kg/(s.kPa)	kg/(s.kPa)
σ_{x_i}	$\pm0.15\times10^{-3}$	$\pm0.15\times10^{-3}$	±0.04	± 0.2	± 2.5	$\pm9.8\times10^{-3}$	± 0.1
Unit	m	m	m s-1	°C	kPa	kPa	kPa

Therefore, the input mass flow rate uncertainties propagation is $\sigma_{\dot{m}} = \pm 2.27 \times 10^{-4}$ kg/s.

REFERENCES

ASME, 2004, ASME Standard MFC-3M-2004, Measurement of fluid flow in pipes using orifice, nozzle and Venturi.

Aronson, R.B., 1976, Vortex tube: cooling with compressed air. Mach. Des. Vol. 48, pp. 140-143.

Awais, M., and Bhuiyan, A.A., 2018, Heat transfer enhancement using different types of vortex generators (VGs): A review on experimental and numerical activities. Therm. Sci. Eng. Prog. Vol. 5, pp. 524-545. https://doi.org/10.1016/j.tsep.2018.02.007.

Bakhsheshi, M.F., Wang, Y., Keenliside, L., and Lee, T., 2016, A new approach to selective brain cooling by a Ranque-Hilsch vortex tube. Intens. Care Med. Exp. Vol. 4, 32. https://doi.org/10.1186/s40635-016-0102-5.

Baz, A., and Uhler, D., 1986, A compressed gas-powered heating system for underwater divers. Ocean. Eng. Vol. 13, pp. 273-290. https://doi.org/10.1016/0029-8018(86)90019-3.

Bruno, T.J., 1994, Chromatographic cryofocusing and cryotrapping with the vortex tube. J. Chromatogr. Sci. Vol. 32, pp. 112-115. https://doi.org/10.1093/chromsci/32.3.112.

Borgnakke, C., and Sonntag, R.E., 2019, Fundamentals of thermodynamics, tenth ed. John Wiley & Sons, Hoboken.

Finko, V.E., 1983, Cooling and condensation of a gas in a vortex flow. Sov. Phys. Tech. Phys. Vol. 28, pp. 1089-1093.

French, F.W., Gilden, G.J., and Nigro Jr., A.R., 2010, Method and system for providing cooling of components in a data storage system. Patent US 7751188 B1.

Gerhart, A.L., and Gerhard, P.M., 2005, Laboratory scale steam power plant study – Rankine cycler™ effectiveness as a learning tool and its component losses. In: Proceedings of the 2005 American Society for Engineering Education Annual Conference and Exposition. Portland, Oregon.

Hilsch, R., 1946, Die Expansion von Gasen im Zentrifugalfeld als Kälteprozeβ. Z. Naturf. Vol. 1, pp. 208–214. https://doi.org/10.1515/zna-1946-0406.

Kleiber, M., and Joh, R., 2010, Properties of pure fluid substances. Chapter D3.1. In VDI e V. (ed.) VDI Heat Atlas, second ed. Springer, Berlin, pp. 301–393.

Kuehn, T.H., Ramsey, J.W., and Threlkeld, J.L., 1998, Thermal environmental engineering, third ed. Prentice Hall, Upper Saddle River.

Linderstrøm-Lang, C.U., 1964, Gas separation in the Ranque-Hilsch vortex tube. Int. J. Heat Mass. Transf. Vol. 7, pp. 1195-1206. https://doi.org/10.1016/0017-9310(64)90061-4.

Liu, J., and Chou, Y.K., 2007, On temperatures and tool wear in machining hypereutectic Al–Si alloys with vortex-tube cooling. Int. J. Mach. Tool. Manu. Vol. 47, pp. 635–645. https://doi.org/10.1016/j.ijmachtools.2006.04.008.

Qyyum, M.A., Wei, F., Hussain, A., Noon, A.A., and Lee, M., 2018, An innovative vortex-tube turbo-expander refrigeration cycle for performance enhancement of nitrogen-based natural-gas liquefaction process. Appl. Therm. Eng. Vol. 144, pp. 117-125. https://doi.org/10.1016/j.applthermaleng.2018.08.023

Rafiee, S.E., 2023, Increasing the heating value of natural gas by reducing CO2 concentration using vortex tube: A new method. Fuel. Vol. 338, 127301. https://doi.org/10.1016/j.fuel.2022.127301.

Ranque, G.S., 1934, Method and apparatus for obtaining from alpha fluid under pressure two currents of fluids at different temperatures. Patent US 1952281 A.

Reader-Harris, M.J., and Sattary, J.A., 1996, The orifice plate discharge coefficient equation – the equation for ISO 5167-1. In: 14th North Sea Flow Measurement Workshop, East Kilbride, Glasgow.

Reader-Harris, M.J., 1998, The equation for the expansibility factor for orifice plates. In: FLOMEKO 98. Lund, Sweden.

Simões-Moreira, J.R., 1999, A thermodynamic formulation of the psychrometer constant. Meas. Science and Technol. Vol. 10, pp. 302-311. https://doi.org/10.1088/0957-0233/10/4/008.

Simões-Moreira, J.R., 2010, An air-standard cycle and a thermodynamic perspective on operational limits of Ranque–Hilsh or vortex tubes. Int. J. Refrig. Vol. 33, pp. 765-773. https://doi.org/10.1016/j.ijrefrig.2010.01.005.

Sharp, P.E., Markwood, W.R. Bletzacker DF., 1966, Cooling system utilizing a Ranque Tube. Patent US 3277238 A.

Stone, W.G., and Love, T.A., 1950, An experimental study of the Hilsch tube and its possible application to isotope separation. Oak Ridge National Laboratory. Report no. ORNL-282.

Sun LabTek, 2022, Lab Equipments, https://sunlabtech.com/mechanical-engineering-lab-equipment/refrigeration-and-air-conditioning-lab-equipment/ (accessed 23 November 2022).

Terekhin, A.A., and Zolotykh, I.K., 2015, Evaporator system of water desalination based on Ranque-Hilsch vortex effect. Procedia Eng. 129, pp. 337-343. https://doi.org/10.1016/j.proeng.2015.12.073.

Wilke, C.R., 1950, A viscosity equation for gas mixtures. J. Chem. Phys. Vol. 18, pp. 517-519. https://doi.org/10.1063/1.1747673.

Wong, G.S.K., and Embleton, T.F.W., 1984, Variation of specific heats and of specific heat ratio in air with humidity. J. Acoust. Soc. Am. Vol. 76, pp. 555-559. https://doi.org/10.1121/1.391597.

Yun, J., Kim, Y., and Yu, S., 2018, Feasibility study of carbon dioxide separation from gas mixture by vortex tube. Int. J. Heat Mass. Tran. Vol. 126, pp. 353-361.

https://doi.org/10.1016/j.ijheatmasstransfer.2018.04.150.

Zavaleta-Aguilar, E.W., Narváez-Romo, B., and Simões-Moreira, J.R., 2023, Ranque-Hilsch vortex tube as an educational tool for classical thermodynamics teaching: research data, Mendeley Data, v1. https://doi.org/10.17632/8zktfd9k9n.1.

Zhai, X., 2017, Research on the application of vortex tube type of cooling jacket in coal mine. AIP Conf. Proc. Vol. 1864, 020220. https://doi.org/10.1063/1.4993037.